Heat Loss Effects on Thin-Channel Detonation Propagation in Hydrogen–Oxygen–Argon Mixtures

Brian Maxwell[1,2], Curran Schmitt[2], Joshua Smith[2]
[1]Department of Mechanical Engineering, University of Ottawa, Ottawa, ON, Canada
[2]Department of Mechanical and Aerospace Engineering, Case Western Reserve University, Cleveland, OH, USA

1 Introduction

To date, several key challenges remain in the understanding and prediction of detonation behaviour, especially in the presence of confining geometry. Fuel safety considerations and the development of detonation-based propulsion systems motivate the importance of research in this field. For example, it is well known that the survivability of detonation wave diffraction from abrupt area changes correlates to the characteristic mixture cell-size [1]. In terms of rotating detonation engine (RDE) development, one key aspect, and perhaps the least understood, is the influence of combustor geometry on engine performance. In this regard, empirical correlations based on the characteristic cell size have been proposed [2] to determine *minimum* functional RDE combustion chamber dimensions. However, optimal geometry considerations to minimize losses and maximize performance have not yet been developed. To complicate matters, a vast majority of RDE experiments have reported a wide range of detonation *velocity deficits*, well below their theoretical Chapman-Jouguet (CJ) solution. In some cases, velocity deficits up to 60% below the CJ-solution have been observed [3]. In fact, such velocity deficits are known to correlate with the lengthening of the reaction structure [4], and likely the cell size as well [5]. This highlights a significant deficiency of using the cell size as a design guideline, without first understanding the influence of momentum and heat losses on the detonation structure from a fundamental perspective.

Although a large number of numerical simulations have been attempted over the years to better understand detonation wave propagation behaviour, extensive numerical simulation efforts [6, 7] have shown that the simulated detonation cells tend to be smaller than those measured experimentally from narrow channels. To clarify such inconsistency between numerics and experiments in terms of detonation cell sizes, one school of thought [7–9] points out the potentially significant role of detailed chemistry and non-equilibrium effects. On the other hand, the work of Maxwell et al. [10] suggested that high rates of turbulent mixing had a direct influence on the hydrodynamic thickness of the detonation structure and its cell size. More recent work of Xiao and Weng [11] has explicitly demonstrated the effect of losses on detonation cell sizes, particularly near the propagation limit, due to the significantly increased detonation velocity deficits resulting in the notably lengthened detonation reaction zones. Such detonation characteristic length scale dependence on losses has also been shown earlier by Radulescu et al. [12, 13] in their slowly diverging channel experiments, which follows the exponential relationship governed by the mixture's effective activation energy. The effect of momentum losses on the detonation velocity and structure, resulting from the presence of boundary layers in thin channels, was further investigated by Maxwell and Wang using viscous three-dimensional simulations with turbulence closure [14]. Very likely, non-equilibrium effects and global perturbations to the flow field resulting from thermal and momentum losses all act to lengthen the detonation cell structure, and velocity deficits likely arise due to the need to conserve momentum and energy in the presence of such losses.

Correspondence to: bmaxwell@uottawa.ca

In the last few years, to account for the presence of losses, Xiao et al. [15] proposed to model the effect of boundary layers on argon-diluted hydrogen-oxygen detonations propagating in thin channels by including an equivalent mass divergence in the lateral direction, akin to Fay's methodology of modeling boundary layer losses [4]. In their model, which employed two-step chemistry, the Mirels' compressible laminar boundary layer theory [16] was adopted for quantifying the boundary-layer-induced loss. Such a formulation has been shown to reproduce the cellular dynamics observed experimentally across a range of initial mixture pressures. This model was later improved by Zangene et al. [17] by including advection of a shock time variable. More recently, Smith et al. [18] further improved the approach by including a detailed elementary reaction mechanism, which required only minimal calibration of the equivalent mass divergence model parameters, and permitted the investigation of marginal detonation propagation behaviour at the most critical pressures. This approach was found useful to speculate on the roles of transverse detonations in sustaining the wave on the verge of propagation failure. To date, these studies show that the influence of boundary losses on the detonation structure and propagation velocity are well understood. In the current paper, we further expand on this approach of two-dimensional modelling using source terms to better understand how the thermal boundary condition and friction separately influence the thin-channel detonation propagation.

2 Mathematical Formulation

Owing to the notorious difficulty and expense in solving the full three-dimensional Navier-Stokes equations for multi-component compressible reactive flows, the much simpler two-dimensional Euler equations were instead solved. We thus consider the conservation of mass, momentum, total energy, and the mass of the kth chemical species:

$$\frac{\partial \rho}{\partial t} + \underline{\nabla} \cdot (\rho \underline{u}) = 0 \tag{1}$$

$$\frac{\partial (\rho \underline{u})}{\partial t} + \underline{\nabla} \cdot (\rho \underline{u} \otimes \underline{u}) + \underline{\nabla} p = \underline{f} \tag{2}$$

$$\frac{\partial (\rho E)}{\partial t} + \underline{\nabla} \cdot ((\rho E + p) \underline{u}) = \dot{q}_L \tag{3}$$

$$\frac{\partial (\rho Y_k)}{\partial t} + \underline{\nabla} \cdot (\rho Y_k \underline{u}) = \dot{\omega}_k. \tag{4}$$

Here, ρ, $\underline{u}$, p, Y_k, and $\dot{\omega}_k$ are the density, velocity vector, pressure, mass fraction of the kth species, and net rate of production of the kth species respectively. The hydrogen portion of the San Diego reaction mechanism [19] was implemented in this study, with 9 species and 23 reversible elementary reactions. The source terms, $\underline{f}$ and $\dot{q}_L$, were appended to the momentum and energy equations, respectively, to account for the momentum and energy losses due to the confining geometry in the third dimension.

For the formulation of the source terms, $\underline{f}$ and $\dot{q}_L$ are based on the one-dimensional model from Xiao and Weng [20], though this model is markedly different. The basis of this model is to compute $\underline{f}$ and $\dot{q}_L$ using an appropriate skin-friction coefficient c_f, i.e. $f_i = \tau_{w,x_i}/L_{c,i} = -\frac{1}{2} c_{f,i} \rho u_i |u_i| / L_{c,i}$, where τ_{w,x_i} is the wall shear stress acting in the x_i direction, and $L_{c,i} = A_i/P_i$ is the characteristic length in the x_i direction, with A_i being the channel cross sectional area in the x_i direction, and P_i being the perimeter of the cross section. For the thin channels studied in this work, we take $L_{c,i} \approx w/2$ in all directions, where w is the width of the channel in the third dimension. The choice of skin-friction correlation in this work is the most significant departure of this model from that of Xiao and Weng [20], who used the fully-developed turbulent boundary layer skin-friction coefficient from Kitano et al. [21], where c_f was taken as $0.38\mathrm{Re}^{-1/4}$. We note that this correlated value is in fact closer in magnitude to the Blasius correlation for the turbulent Darcy friction factor, i.e. $f = 0.316\mathrm{Re}^{-1/4}$, not the skin-friction coefficient.

In our new approach, we instead view the likely undeveloped flow behind the leading shock wave from the perspective of the entrance length problem in duct flows. Moreover, since the boundary layer development is believed to be laminar [13], we therefore instead use the correlation from Shah [22] for an apparent skin-friction coefficient in the entrance region of a duct:

$$c_{f,i} = \frac{1}{\mathrm{Re}_{D,i}} \left(\frac{3.44}{\sqrt{\zeta_i}} + \frac{(c_f \mathrm{Re}_D) + \frac{K(\infty)}{4\zeta_i} - \frac{3.44}{\sqrt{\zeta_i}}}{1 + \frac{C}{\zeta_i^2}} \right), \tag{5}$$

where $\zeta_i = (\Delta x_i / D_H)/\mathrm{Re}_{D,i}$ and is a dimensionless distance, where Δx_i is the distance in the x_i direction of an element that has traveled from its unshocked positions, and $(c_f \mathrm{Re}_D)$, $K(\infty)$, and C are geometry-dependent coefficients based on the cross section of the pipe. For a rectangular channel, these coefficients also depend on the aspect ratio, AR. By interpolation of data provided by Shah [22], for $AR = 0.095$ corresponding to past experiments [15], we take $(c_f \mathrm{Re}_D) = 21.659$, $K(\infty) = 0.796$, and $C = 5.13 \times 10^{-5}$. The hydraulic diameter used to calculate the Reynolds number is approximated for the thin channel as $D_H \approx 2w$. In order to calculate Δx_i in each direction, additional transport equations are included, which carry the initial location of each fluid element, $x_{0,i}$, in a Lagrangian sense, for each i^{th} direction. The spatial displacement term Δx_i can then be calculated by subtracting the advected initial position value, $x_{0,i}$, from the fluid's current lab-frame location, x_i, where $\Delta x_i = |x_i - x_{0,i}|$. Finally, it is important to note that the skin friction correlation of Equation (5) is only valid in the entrance region of the flow. In this study, however, it was assumed that the entrance length was likely much longer than the distance to the sonic plane. Therefore, fully-developed correlations for c_f were not used.

The volumetric heat transfer source term $\dot{q}_L$ is a two-dimensional extension of that used by Xiao and Weng [20]. We assume the total heat transfer through the channel wall in the third dimension is driven by a linear combination of heat transfer carried by convection in both the x- and y-directions, i.e. $\dot{q}_L = \beta \sum_i \dot{q}_{L,i}$, where $\dot{q}_{L,i} = h_{c,i}(T_w - T)/L_{c,i}$. The heat transfer coefficient $h_{c,i}$ is assumed to be governed by the Reynolds analogy in each direction, where the underlying mechanism of heat and momentum transport are the same [23], i.e. $h_{c,i} \approx \frac{1}{2} c_{f,i} c_p \rho |u_i|$. Finally, β is a calibration parameter, which allows implementation of boundary conditions between the adiabatic ($\beta = 0$) and isothermal ($\beta = 1$) extremes.

3 Computational Domain and Initial & Boundary Conditions

Five different pressures and two different mixtures (2 H_2 + O_2 + 2 Ar and 2 H_2 + O_2 + 7 Ar) were studied in this work using three different resolutions ($390.6\,\mu\mathrm{m}$, $195.3\,\mu\mathrm{m}$, and $97.7\,\mu\mathrm{m}$) in an attempt to numerically replicate the experimental work of Xiao et al. [15], as summarized in Table 1. A tree-based adaptive mesh refinement scheme using Cartesian grids was adopted in order to increase computational efficiency by only regions of interest to be captured with high resolution, such as shocks and reaction zones, while allowing lower mesh resolution in the rest of the domain. See Smith et al. [18] for details. A $9.0\,\mathrm{m}$ by $0.2\,\mathrm{m}$ domain was considered. Symmetry boundary conditions were applied to the top, bottom, and left boundaries. The right boundary was given a zero-gradient boundary condition. The quiescent fluid ($x > 4\Delta_\mathrm{i}$) was given an initial temperature of $300\,\mathrm{K}$ and an initial pressure p_0. The first four induction lengths upstream of the detonation front, ($0 < x \leq 4\Delta_\mathrm{i}$), were initialized with the same pressure p_0 and a random density perturbation of up to 25% of the quiescent fluid. These density perturbations were intended to encourage detonation cell growth and formation, and to reduce the time required to reach a quasi-steady state. The flow field from $-0.1\,\mathrm{m} < x \leq 0\,\mathrm{m}$ was initialized with an overdriven ZND profile, such that $f = (D/D_\mathrm{CJ})^2 = 1.1$ was used for all simulations. This was helpful to overcome any potential numerical startup errors due to the large initial discontinuity at the detonation front.

Table 1: Theoretical CJ and experimental [11, 15] velocities, induction lengths (Δ_i) calculated using the experimental wave speed, and cells per Δ_i for the various mixtures and grid resolutions studied. $p_0 = 2.1$ kPa is for 2 H_2 + O_2 + 2 Ar; all other initial pressures are for 2 H_2 + O_2 + 7 Ar.

p_0 (kPa)	D_{CJ} (m/s)	D_{exp} (m/s)	Δ_i (mm)	Cells Per Induction Length		
				390.6 µm	195.3 µm	97.7 µm
2.1	1891	1570	19.02	48.7	97.4	194.8
3.1	1594	1211	33.52	85.8	171.6	343.2
4.1	1602	1330	14.40	36.9	73.7	147.5
6.9	1617	1423	4.72	12.1	24.2	48.4
10.3	1628	1498	2.05	5.2	10.5	21.0

4 Effect of Heat Loss on the Detonation Structure

A summary of the outcomes of simulations carried out in this study, in terms of the measured non-dimensional detonation speeds (D/D_{CJ}), is shown in Fig. 1. Here, we show the detonation velocities obtained for the three different resolutions while varying the contribution of heat loss through the β parameter. For all pressures investigated, the detonation velocities prior to failure are found to change by less than 1% between resolutions, for different values of β. For the $p_0 = 3.1$ kPa case, with the lowest measured experimental propagation speed of $(D_{exp}/D_{CJ}) = 0.76$, the critical β at which detonation failure was observed, at $\beta_{fail} = 0.435 \pm 0.005$, was also found to be grid-independent within 1%. For this pressure, the lowest successful detonation speed observed was $(D/D_{CJ}) = 0.804$, which was 5.8% greater than the experimental value. However, for this case we found that it was possible to capture the experimental value of $(D_{exp}/D_{CJ}) = 0.76$ within 1% by scaling c_f by 1.96, for the adiabatic walls condition, without experiencing detonation failure. For the $p_0 = 2.1$ kPa and $p_0 = 4.1$ kPa cases, whose experimental propagation velocities were the same at $(D_{exp}/D_{CJ}) = 0.83$, the lowest velocities obtained from simulation were all within 2.5%. For $p_0 = 2.1$ kPa and $p_0 = 4.1$ kPa, $\beta_{fail} = 0.79 \pm 0.01$ and $\beta_{fail} = 0.85 \pm 0.15$, respectively. For elevated pressures of $p_0 = 6.9$ kPa and $p_0 = 10.3$ kPa, detonation failure was not observed, even with $\beta = 1$ in the extreme isothermal boundary condition limit. In both of these cases, the lowest propagation speeds measured 2.5% and 3.1% higher than the experimental values of $(D_{exp}/D_{CJ}) = 0.88$ and $(D_{exp}/D_{CJ}) = 0.92$, respectively. At all pressures and β values corresponding to successful propagation, the cellular structure was found to be well resolved for all three resolutions. Evidence of this for the $p_0 = 2.1$ kPa and $p_0 = 4.1$ kPa cases is presented in Fig. 2. For these two pressures the cellular structure was also found to correspond in scale to the experimental images of Xiao et al. [11, 15].

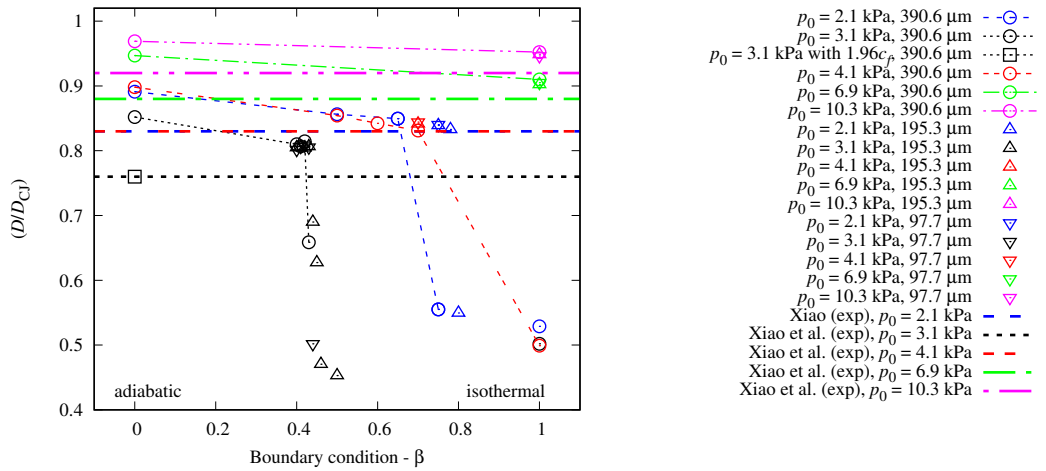

Figure 1: Non-dimensional detonation velocities (D/D_{CJ}) vs. β for all three resolutions (indicated). Also indicated are the experimental speed measurements of Xiao et al. [11, 15]

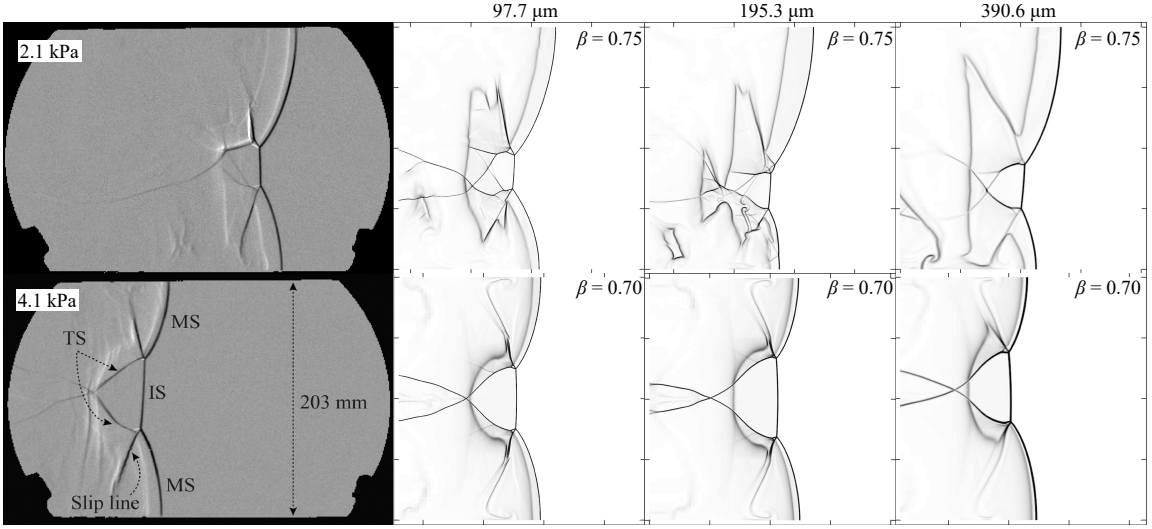

Figure 2: Experimental [11, 15] and numerical schlieren images of detonations at $p_0 = 2.1\,\mathrm{kPa}$ and $p_0 = 4.1\,\mathrm{kPa}$ for various resolutions with the calibrated value of β for each case.

In all cases, at the largest β values that permitted successful detonation propagation, losses due to the skin-friction source term contributed to a larger velocity deficit compared to the heat loss portion. In general, the heat loss portion only accounted for 20% to 41% of the total measured velocity deficit, while skin-friction accounted for the remainder. However, the onset of detonation failure was found to be very sensitive to the presence of heat loss. For example, for detonations with $p_0 = 3.1\,\mathrm{kPa}$ at the $390.6\,\mu\mathrm{m}$ resolution, three different qualitative behaviors were observed for values of β within a very small range: i) successful propagation ($\beta = 0.40$ and 0.41), ii) detonation failure and re-initiation due to marginal behavior ($\beta = 0.42$), and iii) immediate detonation failure with no re-initiation ($\beta = 0.43$). Even though the presence of heat loss, introduced through the β parameter, did not contribute significantly to the overall velocity deficit, it was found to have a large impact on the cellular structure. Figure 3 shows how the presence of heat loss leads to an enlargement of cells compared to the adiabatic case for the $p_0 = 3.1$ kPa and $p_0 = 6.9$ kPa cases. We believe that it is this enlargement of the cellular structure that leads to the marginal behavior and eventual wave failure as the heat loss parameter β is increased.

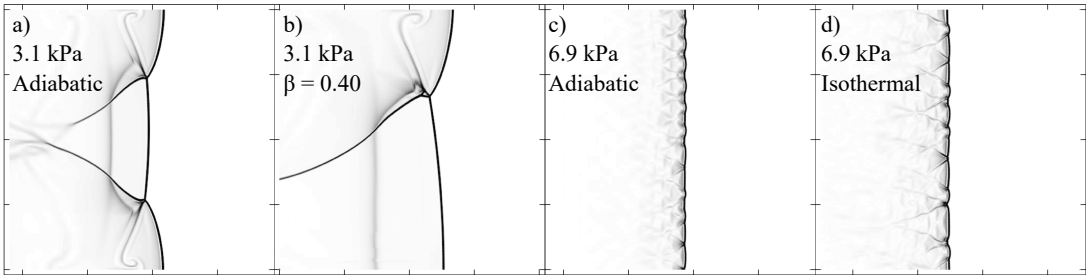

Figure 3: Numerical schlieren images obtained at a resolution of $391\,\mu\mathrm{m}$ for the $p_0 = 3.1\,\mathrm{kPa}$ and $p_0 = 6.9\,\mathrm{kPa}$ cases for adiabatic and either calibrated or isothermal walls.

5 Conclusion

In this work, the proposed momentum and heat-loss model was found to capture the experimentally observed cellular structure and critical velocity deficit within 6%. In general, the heat loss boundary condition, varied through β, contributed only 20% to 41% of the overall velocity deficit, suggesting a

dominance of the momentum losses. This is supported by our previous work [18] where it was demonstrated that experimental velocity deficits were obtainable by considering only the losses resulting from the presence of adiabatic boundary layers, while in this work, detonation failure for $\beta > 0$ generally occurred before the experimental velocity deficits could be reached. We thus suspect that boundary layer momentum losses have a larger impact on the detonation speed compared to heat loss, but that the presence of heat loss can play a significant role in the failure of the wave to propagate.

BM acknowledges support from UL Research Institutes, and also the Natural Sciences and Engineering Research Council of Canada (NSERC), funding reference number RGPIN-2023-03691. JS acknowledges support from the Office of Naval Research grant no. N00014-23-1-2048 (Eric Marineau, program manager). This work made use of the High Performance Computing Resource in the Core Facility for Advanced Research Computing at Case Western Reserve University. The authors are grateful for the input of Q. Xiao, which was valuable to developing the model pursued in this study.

References

[1] Edwards DH, Thomas GO, Nettleton MA (1979). The diffraction of a planar detonation wave at an abrupt area change. J. Fluid Mech. 95: 79–96.

[2] Bykovskii FA, Zhdan SA, Vedernikov EF (2006). Continuous spin detonations. J. Propuls. Power 22: 1204.

[3] Andrus IQ, Polanka MD, King PI, Schauer FR, Hoke JL (2017). Experimentation of premixed rotating detonation engine using variable slot feed plenum. J. Propuls. Power 33: 1448.

[4] Fay JA (1959). Two-dimensional gaseous detonations: Velocity deficit. Phys. Fluids 2: 283.

[5] Monwar M, Yamamoto Y, Ishiii K, Tsuboi T (2007). Detonation propagation in narrow gaps with various configurations. J. Therm. Sci. 16: 283.

[6] Oran ES, Weber JW, Stefaniw EI, Lefebvre MH, Anderson JD (1998). A numerical study of a two-dimensional H_2-O_2-Ar detonation using a detailed chemical reaction model. Combust. Flame 113: 147 .

[7] Taylor B, Kessler D, Gamezo V, Oran E (2013). Numerical simulations of hydrogen detonations with detailed chemical kinetics. Proc. Combust. Inst. 34: 2009 .

[8] Voelkel S, Masselot D, Varghese PL, Raman V (2016). Analysis of hydrogen-air detonation waves with vibrational nonequilibrium. AIP Conf. Proc. 1786: 070015.

[9] Shi L, Shen H, Zhang P, Zhang D, Wen C (2017). Assessment of vibrational non-equilibrium effect on detonation cell size. Combust. Sci. Technol. 189: 841.

[10] Maxwell BM, Bhattacharjee RR, Lau-Chapdelaine SSM, Falle SAEG, Sharpe GJ, Radulescu MI (2017). Influence of turbulent fluctuations on detonation propagation. J. Fluid Mech. 818: 646.

[11] Xiao Q, Weng C (2021). Effect of losses on hydrogen–oxygen–argon detonation cell sizes. Phys. Fluids 33: 116103.

[12] Radulescu M, Borzou B (2018). Dynamics of detonations with a constant mean flow divergence. J. Fluid Mech. 845: 346.

[13] Xiao Q, Radulescu MI (2020). Dynamics of hydrogen–oxygen–argon cellular detonations with a constant mean lateral strain rate. Combust. Flame 215: 437 .

[14] Maxwell B, Wang WH (2023). The influence of boundary conditions on three-dimensional large eddy simulations of calorically perfect gas detonations. Flow Turbul. Combust. 111: 31279.

[15] Xiao Q, Sow A, Maxwell BM, Radulescu MI (2021). Effect of boundary layer losses on 2D detonation cellular structures. Proc. Combust. Inst. 38: 3641.

[16] Mirels H (1956). Boundary layer behind shock or thin expansion wave moving into stationary fluid. Technical Report NACA TN 3712, National Advisory Committee for Aeronautics. URL https://ntrs.nasa.gov/search.jsp?R=19930084483.

[17] Zangene F, Sow A, Radulescu M (2022). Predictability of H2/O2/Ar/He detonations in thin channels: new experiments and improvements in the quasi-two-dimensional mode. In Proceedings of the 28th International Colloquium on the Dynamics of Explosions and Reactive Systems, 175. URL http://www.icders.org/ICDERS2022/abstracts/ICDERS2022-175.pdf.

[18] Smith J, Schmitt C, Xiao Q, Maxwell B (2024). On the nature of transverse waves in marginal hydrogen detonation simulations using boundary layer loss modeling and detailed chemistry. Combust. Flame 268: 113598.

[19] University of California at San Diego (2016). Chemical-kinetic mechanisms for combustion applications. San Diego Mechanism web page, Mechanical and Aerospace Engineering (Combustion Research), University of California at San Diego. URL https://web.eng.ucsd.edu/mae/groups/combustion/mechanism.html.

[20] Xiao Q, Weng C (2023). Unified dynamics of hydrogen–oxygen–diluent detonations in narrow confinements. Fuel 334: 126661.

[21] Kitano S, Fukao M, Susa A, Tsuboi N, Hayashi A, Koshi M (2009). Spinning detonation and velocity deficit in small diameter tubes. Proc. Combust. Inst. 32: 2355 .

[22] Shah R (1978). A correlation for laminar hydrodynamic entry length solutions for circular and noncircular ducts. J. Fluids Eng. 100: 177.

[23] Higgins A (2012). Steady One-Dimensional Detonations, 33–105. Springer Berlin Heidelberg.